Article

Evaluating Shear Strength of Reinforced Concrete Elements Containing Macro-Synthetic Fibers and Traditional Steel Reinforcement

Benedikt Farag , Travis Thonstad , Paolo M Calvi *

Posted Date: 9 September 2025

doi: 10.20944/preprints202509.0760.v1

Keywords: shear strength; macro-synthetic fibers; fiber-steel bars synergy; non-linear analysis; shear design

 doi:10.20944/preprints202509.0760.v1

Article

Evaluating Shear Strength of Reinforced Concrete Elements Containing Macro-Synthetic Fibers and Traditional Steel Reinforcement

Benedikt Farag, Travis Thonstad and Paolo M. Calvi

Department of Civil and Environmental Engineering, University of Washington, Seattle, WA 98195, USA
* Correspondence: pmc85@uw.edu

Abstract

This study investigates the shear behavior of concrete elements reinforced with both traditional steel reinforcement and synthetic fibers, with an emphasis on evaluating the predictive capabilities of current shear design provisions. A review of available experimental data revealed limitations in both quantity and consistency, hindering the formulation of robust design recommendations. To address this, an extensive parametric numerical study was conducted using the VecTor2 nonlinear finite element program, incorporating a recently developed modeling approach for the shear response of macro-synthetic fiber-reinforced concrete (PFRC). A total of 288 simulations were carried out to explore the influence of fiber content, transverse reinforcement ratio, and concrete compressive strength, particularly in ranges not previously captured by experimental programs. The performance of existing design codes, including ACI, CSA, EC2, AASHTO, and the Fib Model Code, was assessed against both experimental data and the enriched parametric dataset. The Fib Model Code demonstrated the most reliable and consistent predictions, outperforming others in terms of both accuracy and low variability. In contrast, the EC2 provisions showed high variability and limited applicability to PFRC. AASHTO provisions displayed reasonable accuracy with respect to both experimental and numerical results. ACI and CSA models were notably conservative across the board. The findings underscore the limitations of current code formulations, particularly at high compressive strengths (≥70 MPa) and highlight the need for design models that better account for synthetic fiber–steel bars interaction and material variability. Future work should focus on expanding the experimental database and developing unified design approaches that explicitly address the synergistic effects of fibers and traditional reinforcement.

Keywords: shear strength; macro-synthetic fibers; fiber-steel bars synergy; non-linear analysis; shear design

1. Introduction

Macro-synthetic fibers are frequently incorporated into concrete mixes to serve as secondary reinforcement. Their main purpose is to help manage cracks caused by shrinkage and temperature variations, while also enhancing the long-term performance of structural components such as bridge superstructures. By improving the tensile properties of concrete, these fibers contribute to greater ductility and more effective crack mitigation. Furthermore, their inherent tensile strength can enhance the overall load-carrying capacity of concrete members (Karthik and Maruthachalam, 2015; AbdelAleem et al., 2018; Joshi et al., 2018; Hossain et al., 2023).

The integration of macro-synthetic fibers presents several advantages for modern construction practices. When used in both precast and cast-in-place elements, they can reduce the need for traditional steel reinforcement, which helps minimize reinforcement congestion. This can lead to

 doi:10.20944/preprints202509.0760.v1

lighter structural elements, finer crack patterns, improved stress distribution, and better confinement at member ends, all of which contribute to improved structural performance.

However, while recognized at a qualitative level, the beneficial contribution of synthetic fibers to the properties macro-synthetic fiber-reinforced concrete (PFRC) is poorly understood and generally neglected in design.

The lack of generalized provisions regarding the use of macro-synthetic fibers as supplemental reinforcement is primarily due to the limited experimental evidence. Particularly scarce is the available experimental evidence pertaining to the shear response of PFRC elements, with even fewer tests focused on investigating the shear behavior of elements reinforced with both macro-synthetic fibers and deformed steel bar (see Figure 1).

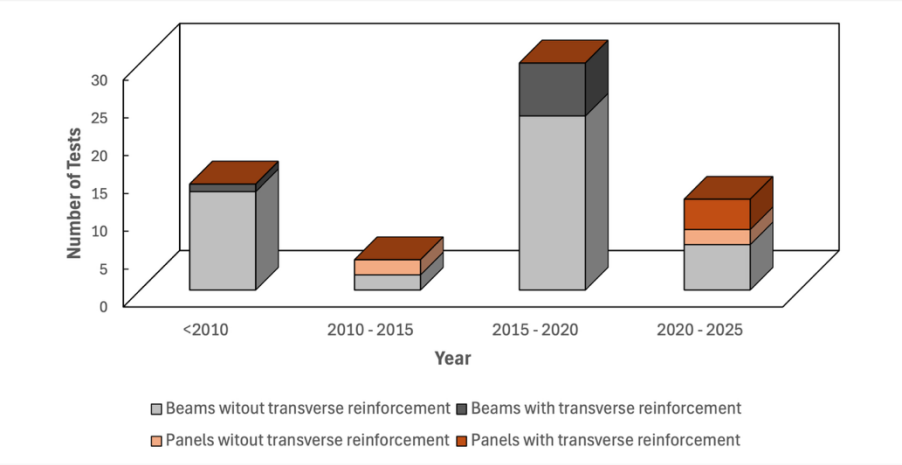

Figure 1. Available PFRC beams and panels from experimental studies in the literature.

Notably, experimental findings on the combined use of deformed steel bars and fiber reinforcement for shear resistance indicate that incorporating fibers into reinforced concrete beams enhances their shear capacity. This enhancement often promotes a shift in failure mode from brittle to more ductile behavior (Swamy & Bahia, 1985; Amin & Foster, 2015; Cucchiara et al., 2004; Aoude et al., 2012; Farag et al., 2024). Despite these promising results, the limited availability of experimental data has prevented the inclusion of specific design provisions for fiber-reinforced concrete with conventional stirrups in current structural design standards.

The primary challenge to advancing design methodologies lies in the difficulty of producing enough experimental data to support the development of robust and widely applicable design equations. Experimental investigations are resource-intensive and often constrained in terms of the number of variables they can evaluate.

To address this limitation, Farag et al. (2024) introduced a nonlinear numerical modeling strategy tailored for synthetic fiber-reinforced concrete elements subjected to shear. Their approach, implemented using the VecTor2 finite element platform (Wong et al., 2013), was calibrated using experimental data provided by Gaston (2023) and validated against a comprehensive collection of panel and beam test results reported in the literature. The study demonstrated a strong alignment between model predictions and observed behavior, with an average predicted-to-measured shear strength ratio of 0.99 and a coefficient of variation of 5.5%.

This modeling framework offers a powerful alternative to physical testing, allowing for extensive simulations across a broad range of parameters and conditions. It helps bridge the data gap and supports the development of rational shear design methodologies by generating reliable insights where physical testing is limited.

This paper contributes to filling that knowledge gap by first reviewing relevant experimental data to evaluate the accuracy of five international design codes. Subsequently, 288 panel specimens are designed and analyzed in VecTor2, covering variables such as concrete compressive strength, fiber dosage, and transverse reinforcement ratio. The resulting database is used to highlight key

 doi:10.20944/preprints202509.0760.v1

behavioral trends and to assess the performance of the selected design provisions, offering critical support for refining design recommendations.

2. Available Experimental Evidence

The shear response of PFRC elements has predominantly been investigated experimentally considering two types of structural components, namely beam tests and panel tests (examples in Figure 2). Beam tests have typically involved simply supported beams subject to three or four-point bending, while the few PFRC panel tests reported in the literature have been conducted using special panel element testers, only available at a few institutions (e.g., University of Toronto, University of Washington).

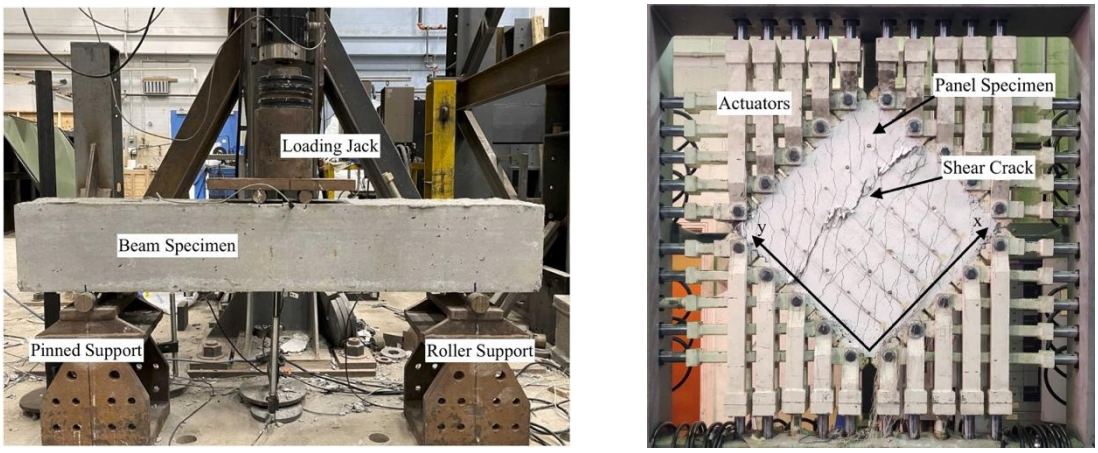

(a) Shear resistance of beam (adapted from Ismail, 2025) (b) Panel Element Tester

Figure 2. Typical experimental setups for PFRC testing.

A number of experimental investigations have explored the shear behavior of polymer fiber-reinforced concrete (PFRC) beams, with a total of 52 beam tests identified in the literature (details provided in Table A1, Appendix). Noteworthy contributions include studies by Greenough and Nehdi (2008), Altoubat et al. (2009), Parmentier et al. (2012), Conforti et al. (2015), Sahoo et al. (2015), Ababneh et al. (2017), Arslan et al. (2017), Murad and Abdel-Jabbar (2022), and Koura et al. (2024). These works collectively examined the effects of key parameters such as beam depth, shear span-to-depth ratio (a/d), reinforcement ratios (both longitudinal ϱ_l and transverse ϱ_t), compressive strength (f'_c), fiber volume fraction (V_f), and fiber length (l_f), as outlined in Table 1.

While PFRC beam testing is relatively well represented, only a limited number of studies have evaluated the combined contribution of macro-synthetic fibers and traditional shear reinforcement. Just 14 such tests (spanning both beam and panel elements) could be identified in the literature (e.g., Majdzadeh et al., 2006; Navas et al., 2018; Bastami, 2019). These investigations suggest that combining macro-synthetic fibers with transverse steel reinforcement can significantly improve shear performance, with reported strength increases ranging from 11% to 47% relative to conventional reinforced concrete (RC) counterparts. In some cases, synergistic behavior has been observed, where the enhancement in shear strength exceeds the sum of the contributions from fibers and stirrups used in isolation. For instance, Majdzadeh et al. (2006) documented a 10% synergistic gain in shear strength in PFRC beams containing 0.5% fiber volume and a transverse reinforcement ratio of 0.28%.

Table 1. Summary of variables tested in PFRC beam experimental programs.

 doi:10.20944/preprints202509.0760.v1

	PFRC Beams without shear reinforcement: 44			PFRC Beams with shear reinforcement: 8		
Parameter	**Max**	**Min**	**Average**	**Max**	**Min**	**Average**
d (mm)	473	120	255	481	120	328
a/d	5.23	1.50	3.12	4.82	3.00	3.93
ρ_l (%)	3.22	0.47	1.85	2.62	1.41	2.06
ρ_t (%)	-	-	-	0.50	0.10	0.28
f'_c (MPa)	78.3	13.9	38.6	91.6	37.8	56.7
V_f (%)	3.00	0.22	1.05	1.10	0.50	0.89
l_f (mm)	54.0	12.5	43.7	50.0	48.0	49.0

In addition to beams, a smaller subset of studies has examined PFRC panels subjected to shear. Carnovale (2013) and Carnovale and Vecchio (2014) reported that macro-synthetic fibers can effectively limit crack widths by bridging cracks, thereby enhancing shear response. However, these studies also found that achieving shear capacity comparable to that of steel fibers required significantly higher fiber volumes. For example, Carnovale (2013) observed that 2.0% macro-synthetic fibers were needed to match the performance of panels reinforced with just 0.5% hooked-end steel fibers. The use of high fiber volumes, however, was also associated with workability challenges.

To contribute to the limited dataset on PFRC elements incorporating both macro-synthetic fibers and conventional shear reinforcement, Gaston (2023) conducted a focused experimental program. Nine panel specimens, six PFRC and three RC, were tested under monotonic pure shear using the Panel Element Tester at the University of Washington. The main variables examined were macro-synthetic fiber volume and transverse reinforcement ratio (ϱ_t), which varied between 0% and 0.91%. The fiber content ranged from 0% to 0.52%, while the longitudinal reinforcement ratio was held constant at 2.28% for all specimens. This ratio was selected to exceed twice the highest transverse reinforcement level to promote shear-dominated failure while minimizing the risk of premature biaxial yielding. With his recent experimental program, a total of 8 PFRC panels were found in the literature with their key properties summarized in Table 2.

Findings from Gaston's study revealed that the shear strength was primarily governed by ϱ_t. The fibers provided measurable benefits in terms of crack width reduction but only modest improvements in strength at the dosage levels tested. Notably, the effectiveness of the fibers was influenced by the amount of shear reinforcement. More pronounced strength gains were observed in panels with lower ϱ_t values. For example, an increase in fiber content from 0.26% to 0.52% resulted in a 15% improvement in shear strength when ϱ_t was 0.34%, whereas the same increase in fiber dosage produced negligible strength gains for specimens with ϱ_t = 0.91%. This trend is consistent with the findings of Navas et al. (2018), where fiber contribution was more substantial at lower reinforcement levels (ϱ_t = 0.10%) and diminished as ϱ_t increased to 0.15%.

Table 2. Summary of variables tested in PFRC panel experimental programs.

	PFRC Panels without shear reinforcement: 4	PFRC Panels with shear reinforcement: 4

 doi:10.20944/preprints202509.0760.v1

Parameter	Max	Min	Average	Max	Min	Average
b (mm)	890	890	890	890	890	890
t (mm)	70	70	70	70	70	70
ρ_l (%)	3.31	2.28	2.80	2.28	2.28	2.28
ρ_t (%)	-	-	-	0.91	0.29	0.60
f'_c (MPa)	54.3	29.4	41.8	45.0	36.1	40.8
V_f (%)	2.00	0.26	1.20	0.52	0.26	0.39
l_f (mm)	54	40	47	40	40	40

3. Current Code-Based Approaches to Estimate Shear Strength

Five major international codes, namely the AASHTO LRFD specifications (AASHTO, 2020), ACI 318 (ACI 2019), the Canadian Standards Association's Design of Concrete Structures (CSA A23.3, 2019), CEB-FIP Model Code 2010 (Fib, 2010), and the Eurocode (Eurocode 2, 2015), were considered in this work. This section provides an overview of the shear provisions contained in these design standards.

3.1. AASHTO LRFD Bridge Design Specifications

The basis for the current shear provisions in the *AASHTO LRFD Bridge Design Specifications* is the Modified Compression Field Theory (MCFT) (Vecchio and Collins, 1986). According to the MCFT, the shear strength of a concrete member can be estimated if two parameters, β and θ, are known. These two factors depend on the longitudinal strain in the element and the crack spacing, and values for β and θ can be computed using closed-form equations, for members with and without transverse reinforcement (Bentz et al., 2006). The *AASHTO LRFD Bridge Design Specifications* do not consider the contribution of fibers to a member's shear strength, rather the nominal shear resistance is determined as the sum of contributions from the concrete, transverse steel, and prestressing:

$$v_n = \min \begin{cases} v_c + v_s + v_p \\ 0.25 f'_c + v_p \end{cases} \quad (1)$$

$$v_c = 0.0316\beta \cdot \sqrt{f'_c} \quad (2)$$

$$v_s = \frac{A_v f_y \cdot (\cot\theta + \cot\alpha)\sin\alpha}{b_v \cdot s} \quad (3)$$

where A_v is the area of transverse reinforcement within a distance s, f'_c is the specified concrete cylinder compressive strength in MPa, f_y is the yield stress of the transverse reinforcement in MPa, b_v is the effective web width, β is a parameter that accounts for the concrete's ability to transmit tensile stresses, θ is the angle of inclination of compressive stress, and α is the angle of inclination of transverse reinforcement. The parameters β and θ are calculated as:

$$\beta = \frac{4.8}{1+750\epsilon_x} \text{ for } A_v \geq 0.083\sqrt{f'_c} \cdot \frac{b_v \cdot s}{f_y} \quad (4)$$

$$\beta = \frac{4.8}{1+750\epsilon_x} \cdot \frac{1300}{1000+s_{xe}} \text{ for } A_v < 0.083\sqrt{f'_c} \cdot \frac{b_v \cdot s}{f_y} \quad (5)$$

$$\theta = 29 + 3500\epsilon_x \quad (6)$$

Where $s_{xe} = s_x \cdot 35/(a_g + 16)$ is the crack spacing parameter as influenced by aggregate size (300 mm $\leq s_{xe} \leq$ 2,000 mm), a_g is the maximum aggregate size for the concrete in millimeters, and the

 doi:10.20944/preprints202509.0760.v1

crack spacing, s_x, is taken as the effective member depth, d_v, or the maximum distance between layers of longitudinal crack control reinforcement, whichever is less. The net longitudinal strain in the section at the centroid of the tensile reinforcement, ϵ_x, is computed as:

$$\epsilon_x = \frac{\frac{|M_u|}{d_v} + 0.5N_u + 0.5|V_u - V_p| - A_{ps}f_{po}}{E_s A_s + E_p A_{ps}} \quad (7)$$

where M_u is the factored moment at the section, N_u is the factored axial force at the section, V_u is the factored shear force at the section, V_p is the component of prestressing force in the direction of the shear force, f_{po} is the effective prestress in the prestressed reinforcement (often taken as $0.7f_{pu}$), and E_s, A_s, E_p, and A_{ps} are the elastic modulus and area of the non-prestressed and prestressed tension reinforcement on the flexural tension side of the member, respectively.

3.2. ACI 318

Although ACI-318 permits the use of SFRC beams without stirrups if certain criteria are met, it does not quantify the contribution of fiber-reinforcement to the strength of structural elements; the shear strength of FRC for non-prestressed members is conservatively assumed equal to that of conventional concrete, like the *AASHTO LRFD Bridge Design Specifications*.

$$v_c = \left[0.66\lambda_s\lambda(\rho_w)^{1/3}\sqrt{f_c'} + \frac{N_u}{6A_g}\right] \quad (8)$$

where N_u is the acting axial force, A_g is the gross area of the cross section, ρ_w is the web longitudinal reinforcement ratio, f_c' is the 28-day cylinder strength in MPa, λ is a factor to account for lightweight concrete, and λ_s is the size effect factor, computed as

$$\lambda_s = \begin{cases} 1.0, & \text{if } A_v \geq A_{v,min} \\ \sqrt{\frac{2}{1+0.004\cdot d}} \leq 1.0, & \text{if } A_v < A_{v,min} \end{cases} \quad (9)$$

The minimum transverse reinforcement ratio $A_{v,min}$ is determined by:

$$A_{\mathrm{v,min}} = \max\left(0.062\sqrt{f'_c}\cdot\frac{b_w}{f_{yt}},\quad 0.35\cdot\frac{b_w\cdot s}{f_{yt}}\right) \quad (10)$$

Where d is the depth of the cross section, b_w is the width of the web of the section, s is the transverse reinforcement spacing and f_{yt} is the yield stress of the transverse reinforcement in psi. The contribution of the transverse reinforcement is computed similarly to the AASHTO and *fib* codes, however ACI 318 assumes an inclination, θ=45°, which simplifies the calculation. ACI 318 imposes an upper limit for the transverse reinforcement strength contribution of $v_s = \rho_y f_{yt} \leq 0.66\sqrt{f'_c}$. The nominal shear strength is thus:

$$v_n = v_c + v_s \quad (11)$$

3.3. CEB-fib Model Code 2010

The fib Model Code 2010 considers the benefit of fibers to the shear strength of concrete, specifying the shear strength contribution of FRC as:

$$v_{Rd,F} = \frac{0.18}{\gamma_c}k\left[100\rho\left(1 + 7.5\frac{f_{Ftuk}}{f_{ctk}}\right)f'_c\right]^{1/3} + 0.15\sigma_{cp} \geq 0.035k^{3/2}\sqrt{f'_c} + 0.15\sigma_{cp} \quad (12)$$

where γ_c is the partial safety factor for concrete (taken as 1.0 for comparison to experimental strengths), σ_{cp} is the compressive stress in the element caused by external loads or prestressing, f'_c is the 28-day compressive cylinder strength in MPa, ρ is the longitudinal reinforcement ratio, $k = 1 + \sqrt{200/d} \leq 2.0$ is a size effect factor that depends on the member depth d (in mm), f_{Ftuk} is the characteristic value of the ultimate residual tensile strength, and f_{ctk} is the characteristic tensile strength. For a crack width at ultimate, w_u=1.5 mm:

$$f_{Ftuk} = f_{Fts} - \frac{w_u}{CMOD_3}(f_{Fts} - 0.5f_{R3} + 0.2f_{R1}) \geq 0 \quad (13)$$

 doi:10.20944/preprints202509.0760.v1

where f_{R1} and f_{R3} are the residual strengths from an FRC flexural test at $CMOD_3$=0.5 mm and $CMOD_3$=2.5 mm, respectively. The residual strengths can be estimated by

$$f_{R3} = 6.0 \cdot \left(V_f \cdot \frac{l_f}{d_f}\right)^{0.7} \quad (14)$$

$$f_{R1} = 7.5 \cdot \left(V_f \cdot \frac{l_f}{d_f}\right)^{0.8} \quad (15)$$

$$f_{Fts} = 0.45 f_{R1}. \quad (16)$$

The characteristic tensile strength f_{ctk} is taken as f_{ctm} according to:

$$f_{ctm} = 0.3(f_{ck})^{2/3} \quad \text{for } f'_c \leq 50 \text{ MPa} \quad (17)$$

$$f_{ctm} = 2.12 \cdot \ln\left(1 + 0.1(f'_c + \Delta f)\right) \quad \text{for } f'_c > 50 \text{ MPa} \quad (18)$$

where Δf =8 MPa. If the transverse reinforcement ratio, $\rho_t > 0.08\sqrt{f'_c}/f_y$, the shear resistance of the member is taken as the sum of concrete and transverse steel contributions:

$$v_{Rd} = v_{Rd,F} + v_{Rd,s} \leq v_{Rd,max} \quad (19)$$

The contribution from the transverse reinforcement and the strength limit are computed by:

$$v_{Rd,max} = k_\epsilon \cdot \frac{f'_c}{\gamma_c} \cdot \sin\theta \ \cos\theta \quad (20)$$

$$v_{Rd,s} = \frac{A_s}{s \cdot b_w} \cdot f_y \cot\theta \quad (21)$$

where $\theta_{\min} \leq \theta \leq 45°$, $\theta_{\min} = 20° + 10\,000\epsilon_x$, and

$$k_\epsilon = \frac{1}{1.2+55\epsilon_1} \leq 0.65 \quad (22)$$

$$\epsilon_1 = \epsilon_x + (\epsilon_x + 0.002)\cot^2\theta \quad (23)$$

The longitudinal strain, ϵ_x, is determined by:

$$\epsilon_x = \frac{1}{2E_s A_s}\left(\frac{M_{Ed}}{z} + V_{Ed} + N_{Ed}\left(\frac{1}{2} - \frac{\Delta e}{z}\right)\right) \quad (24)$$

where M_{Ed}, V_{Ed}, and N_{Ed} are the design moment, shear, and axial load at the section under consideration; Δe is the distance from the section geometric centroid to mid-depth of the effective shear depth; z is the effective shear depth that can be assumed equal to $0.9d$; and E_s and A_s are the elastic modulus and area of the non-prestressed tension reinforcement.

3.4. CSA A23.3 (2019)

The CSA A23.3 is based on the MCFT and is very comparable to AASHTO, with some minor differences. The shear strength is computed from Equation 1, but the concrete contribution is computed from Equation 25.

$$v_c = \lambda\beta\sqrt{f_c'} \quad (25)$$

Where $\sqrt{f_c'} \leq 8\,MPa$ and $\lambda = 1.0$ for normal weight concrete. The steel contribution aligns with AASHTO and is computed according to Equation 3, but coefficients β and θ are determined using the general method as:

$$\beta = \frac{0.4}{1+1500\varepsilon_x}\frac{1300}{1000+s_{ze}} \geq 0.05 \quad (26)$$

$$\theta = 29 + 7000\varepsilon_x \quad (27)$$

$$\varepsilon_x = \frac{M_f/d_v + V_f}{2E_s A_s} \quad (28)$$

 doi:10.20944/preprints202509.0760.v1

Where V_f and M_f are the design shear and moment, respectively, and d_v is the effective shear depth. The equivalent crack spacing parameter is $s_{ze} = 300\,mm$ for sections with minimum transverse reinforcement that satisfy Equation 29:

$$A_v \geq 0.06\sqrt{f_c'}\frac{b_v s}{f_{yt}} \qquad (29)$$

But:

$$s_{ze} = s_z \frac{35}{a_g + 15} \qquad (30)$$

For sections without minimum transverse reinforcement, whichever is less. Additionally, for compressive strengths $f_c' \geq 70MPa$, $a_g = 0$ should be used in Equation 10. As f_c' goes from 60 MPa to 70 MPa, a_g shall be linearly reduced to zero.

3.5. Eurocode 2 (EC2)

The EC2 provides two approaches to compute the shear resistance of members with and without transverse reinforcement, respectively.

For members without transverse reinforcement the shear resistance is computed as

$$v_{Rd,c} = C_{Rd,c}k(100\rho_l f_{ck})^{1/3} + k_1\sigma_{cp} \geq v_{min} + k_1\sigma_{cp} \qquad (31)$$

Where:

$k = 1 + \sqrt{200/d} \leq 2$

$\rho_l = A_{sl}/(b_w d) \leq 0.02$ (A_{sl} is the area of tensile reinforcement)

$\sigma_{cp} = N_{Ed}/A_c$ where N_{Ed} is the axial force on the cross section and A_c is area of concrete cross section. The minimum shear strength is computed as:

$$v_{min} = 0.035k^{3/2}{f_{ck}}^{1/2} \qquad (32)$$

And the recommended values for $C_{Rd,c}$ and k_1 are $0.18/\gamma_c$ and 0.15 respectively.

The strength of members containing shear reinforcement is computed as the minimum of two contributions, namely $v_{Rd,s}$ and $v_{Rd,max}$. The term $v_{Rd,s}$ represents the strength of the transverse reinforcement, while the term $v_{Rd,max}$ represents the crushing strength of the concrete struts:

$$v_{Rd,s} = \frac{0.9 \cdot A_{sw} f_{yt}}{b \cdot s} \cdot cot\,\theta \qquad (33)$$

$$v_{Rd,max} = \alpha_{cw} \cdot 0.9 \cdot v_1 \cdot \frac{f_{cd}}{cot\,\theta + tan\,\theta} \qquad (34)$$

$$v_{Rd} = \min(v_{Rd,s}, v_{Rd,max}) \qquad (35)$$

And $\alpha_{cw} = 1$ for non-prestressed members, $z = 0.9d$ and

$$v_1 = \begin{cases} 0.6, & f_{ck} \leq 60MPa \\ 0.9 - \dfrac{f_{ck}}{200} > 0.5, & f_{ck} > 60MPa \end{cases} \qquad (36)$$

$$f_{cd} = f_{ck}/\gamma_c \qquad (37)$$

In the equations above, $\gamma_c = 1.0$ and the angle θ is such that $1 \leq cot\,\theta \leq 2.5$ ($21.8 \leq \theta \leq 45\,deg$), which is the range permitted by EC2.

4. Available Design Methods Reliability Assessment

To evaluate the precision and reliability of the shear design methods described in Section 3, predicted-to-experimental strength ratios were compared for four categories of PFRC specimens sourced from the literature: beams without shear reinforcement, beams with shear reinforcement, panels without shear reinforcement, and panels with reinforcement. The spread of these predicted-to-experimental strength ratios is illustrated in Figure 3, while Table 3 provides a summary of the

 doi:10.20944/preprints202509.0760.v1

average, median, and coefficient of variation (COV) values for each design model within each category. A ratio of 1.0 indicates perfect agreement between predicted and experimental values; deviations reflect underestimation (<1.0) or overestimation (>1.0).

In the following of this section, each model's performance is evaluated based on its proximity to the 1.0 benchmark and the variability of the data, reflecting both accuracy and reliability. A separate discussion is provided for the individual groups of specimens.

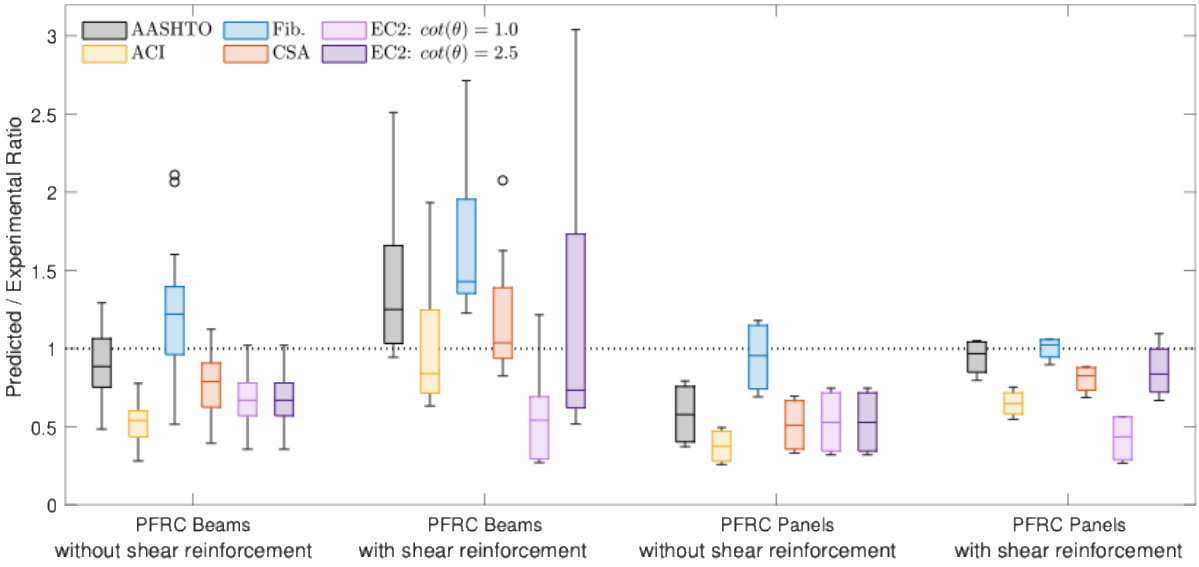

Figure 3. Performance assessment of shear design codes against available experimental evidence.

For PFRC Beams without Shear Reinforcement, the AASHTO model yielded the most accurate predictions with a mean and median average strength ratio of 0.90 and 0.89, respectively, and relatively low scatter (Cov = 22.0%), suggesting consistent performance.

The Fib Model Code also exhibited reasonable performance, with an average ratio of 1.20 and median of 1.22, indicating overprediction but good alignment with experimental values. Its coefficient of variation is 28.8%.

ACI and CSA models underpredicted shear strength more markedly (Avg = 0.52 and 0.77, respectively), while maintaining reasonable consistency (Cov ≈ 22–23%). Both **EC2 variants** also underpredicted strength with similar averages (0.68), and consistency (Cov = 22.5%).

With the introduction of shear reinforcement in beams, variability increased across most models. The Fib model again produced the highest average (1.68) and median (1.43) values. The AASHTO model also overpredicted (Avg = 1.42), though with a relatively large spread (Cov = 38.7%), suggesting reduced consistency compared to unreinforced cases.

In contrast, ACI and CSA models delivered moderate predictions (Avg = 1.02 and 1.20), but their medians (0.84 and 1.04) and high coefficients of variation (Cov = 44.5% and 35.6%) reveal considerable dispersion in results. Notably, EC2 with cot(θ) = 1.0 significantly underestimated shear capacity (Avg = 0.57), with the highest variability among all models (Cov = 56.3%). The cot(θ) = 2.5 variant achieved an average of 1.22 but suffered from extremely high scatter (Cov = 74.0%), indicating unreliable predictions.

The performance of all models deteriorated when applied to PFRC panels without shear reinforcement. The Fib Model Code performed best (Avg = 0.95, Med = 0.95, Cov = 25.4%), demonstrating high accuracy and relatively low dispersion. However, AASHTO, ACI, and CSA were all notably conservative, with average ratios of 0.58, 0.38, and 0.51, respectively. The ACI model showed the lowest mean of all (0.38), though with moderate variability (Cov = 30.2%).

Both EC2 models produced identical averages (0.53) and medians, accompanied by high variability (Cov = 41.0%).

 doi:10.20944/preprints202509.0760.v1

Finally, for PFRC Panels with shear reinforcement, the AASHTO and Fib models again provided the most satisfactory predictions, with average ratios of 0.95 and 1.00, and coefficients of variation under 15%, indicating good alignment and reliability. CSA and ACI remained conservative (Avg = 0.81 and 0.65, respectively), with a similar consistency compared to other groups.

The EC2 model with cot(θ) = 1.0 continued to underpredict (Avg = 0.43), while EC2 cot(θ) = 2.5 yielded an average closer to unity (0.86).

Table 3. Performance of shear design codes against experimental evidence (predicted/experimental).

	PFRC beams without shear reinf.			**PFRC beams with shear reinf.**			**PFRC panels without shear reinf.**			**PFRC panels with shear reinf.**		
	Avg	**Med**	**Cov (%)**	**Avg**	**Med**	**Cov (%)**	**Avg**	**Med**	**Cov (%)**	**Avg**	**Med**	**Cov (%)**
AASHTO	0.90	0.89	22.0	1.42	1.25	38.7	0.58	0.58	35.9	0.95	0.97	12.7
ACI	0.52	0.54	22.7	1.02	0.84	44.5	0.38	0.37	30.2	0.65	0.65	13.6
Fib.	1.20	1.22	28.8	1.68	1.43	31.8	0.95	0.95	25.4	1.00	1.02	7.6
CSA	0.77	0.79	22.7	1.20	1.04	35.6	0.51	0.51	35.5	0.81	0.83	11.4
EC2: cot(θ)=1.0	0.68	0.67	22.5	0.57	0.54	56.3	0.53	0.53	41.0	0.43	0.44	37.4
EC2: cot(θ)=2.5	0.68	0.67	22.5	1.22	0.73	74.0	0.53	0.53	41.0	0.86	0.84	21.3

The results outlined above show that, overall, the Fib Model Code tends to yield the most balanced and reliable strength predictions across all specimen types, followed by the AASHTO model which also performs well compared to the other codes tested. ACI and CSA models are generally overly conservative.

While the EC2 model with cot(θ) = 1.0 offers safe lower-bound estimates, its applicability appears limited by persistent underprediction. The cot(θ) = 2.5 variant suffers from high dispersion, especially for beams with shear reinforcement.

Crucially, no single model emerged as consistently reliable across both beams and panels with shear reinforcement (which represent the focus of this work). The Fib Model Code, despite offering accurate predictions in reinforced panels (Avg = 1.00, Cov = 7.6%), tended to overestimate shear strength in reinforced beams (Avg = 1.68). Similarly, the AASHTO model, though generally reasonable, displayed notable variability in reinforced beams (Cov = 38.7%). Models such as ACI, CSA, and the EC2 variants showed either persistent underprediction or unacceptable scatter, particularly in the case of EC2 with cot(θ) = 2.5, which had the highest coefficient of variation (Cov = 74.0%) among all.

These findings underscore that the model reliability decreases in the presence of shear reinforcement. The interaction between fibres and traditional transverse steel is more complex and less well understood in current design formulations.

Importantly, this assessment is based on a limited dataset extracted from the available experimental literature. While trends can be observed, the statistical robustness of the conclusions is constrained by the small sample sizes and variability in test configurations, materials, and loading protocols. As such, additional data are essential to develop a more statistically representative

 doi:10.20944/preprints202509.0760.v1

evaluation of model performance. This would enable not only a more refined calibration of existing models but also the potential development of new approaches better suited to the hybrid behavior of fibre-reinforced concrete with shear reinforcement. This identified gap provides the motivation for the work conducted herein and presented in the remainder of this paper.

5. Generation of a Comprehensive Database of Shear Results via Numerical Analyses

The results presented in the previous sections have shown that limited experimental evidence pertaining to the response of PFRC structural components exists in the literature, complicating the identification/development of definitive shear design recommendations. The limited results analysed in Section 4 suggest that the Fib Model Code may be best suited to be adopted or adapted for use in this context, however limitations were identified, and it was discussed how definitive recommendations can only be made considering more conclusive evidence. It was noted that there are only a handful of specimens tested in the literature that contain both synthetic fibers and traditional steel reinforcement.

Evidently, it is difficult to generate an amount of experimental data that is statistically meaningful to support the adoption of a given design methodology or the implementation of a new approach, and each experimental program can only focus on a limited number of variables. In contrast, large shear databases can be generated via numerical analysis, provided that reliable modeling strategies are available to simulate the response of selected specimens.

To this end, a numerical modeling approach for PFRC elements subjected to shear was recently proposed by Farag et al. (2024) and implemented in the finite element software VecTor2 (Wong et al., 2013). This was used herein to conduct an extensive parametric study to extend the results of the available experimental testing programs, exploring additional combinations of parameters, and to generate results that are used in later sections to further assess the reliability of the design provisions summarized in Section 3.

The case study structures considered in the parametric study consisted of PFRC panels with baseline properties (e.g., geometry and loading conditions) identical to the specimens tested experimentally by Gaston (2023), encompassing a wide range of PFRC specimens varying in concrete compressive strength (20 MPa to 95 MPa), fibre volume fraction, and shear span-to-depth ratios. Panel specimens were selected at this stage to set some limits to the number of variables at play, and to narrow the scope to studying elements in pure shear. Additionally, while the model proposed by Farag et al. is believed to be reliable to simulate the response of beam elements, it was formulated and calibrated specifically to deal with panel/membrane type structural components. Hence, there is a higher degree of confidence placed on the ability of the simulator to accurately replicate the behavior of panel type specimens, which further motivated the decision to generate a numerical database of panel test results.

Details pertaining to the parametric study conducted are provided in the following subsections, including a discussion of the key outcomes and main trends observed as a function of the different variables considered.

5.1. Case study Structures Definition and Numerical Modeling

The recently developed modeling strategy by Farag et al. (2024) introduced earlier enables the generation of extensive numerical datasets that can be utilized to critically evaluate the performance of existing shear design provisions. Thus, a total of 288 PFRC panel configurations were simulated, systematically varying key design variables including concrete compressive strength (ranging from 20 MPa to 95 MPa), transverse reinforcement ratio (ρ_t from 0% to 1.5%), and macro-synthetic fiber content (V_f from 0% to 2%). These parameters were chosen to encompass both typical and boundary-case values that may arise in practical applications, allowing the influence of individual and combined effects to be fully explored. In particular, the combination of these variables allowed identification of design regimes where fiber addition may be most effective.

 doi:10.20944/preprints202509.0760.v1

All specimens analyzed in this parametric study share a consistent geometry of 1000 mm × 1000 mm × 70 mm, matching common panel sizes in experimental programs (e.g., Carnovale, 2013; Zhang et al., 2020; Gaston, 2023). The longitudinal reinforcement ratio (ϱ_x) was fixed at 2.28%, a value exceeding the maximum considered ϱ_t by approximately 50%, ensuring shear-dominated behavior and avoiding the development of biaxial yielding. Uniform shear loads were applied incrementally to simulate monotonic loading up to failure. The complete matrix of test parameters is outlined in Table 4.

Table 4. Variables considered in the numerical parametric study.

f'_c (MPa)	V_f (%)	ρ_t (%)	Dimensions (mm x mm x mm)	ρ_x (%)	Loading
20	0, 0.25, 0.5, 0.75, 1.0, 1.25, 1.5, 1.75, 2.0	0, 0.1, 0.25, 0.5, 0.75, 1.0, 1.25, 1.5	1000 x 1000 x 70	2.28	Uniform shear
45	0, 0.25, 0.5, 0.75, 1.0, 1.25, 1.5, 1.75, 2.0	0, 0.1, 0.25, 0.5, 0.75, 1.0, 1.25, 1.5			
70	0, 0.25, 0.5, 0.75, 1.0, 1.25, 1.5, 1.75, 2.0	0, 0.1, 0.25, 0.5, 0.75, 1.0, 1.25, 1.5			
95	0, 0.25, 0.5, 0.75, 1.0, 1.25, 1.5, 1.75, 2.0	0, 0.1, 0.25, 0.5, 0.75, 1.0, 1.25, 1.5			

The numerical simulations were performed using VecTor2 (Wong et al., 2013), a nonlinear finite element platform based on the Modified Compression Field Theory (Vecchio and Collins, 1986) and the Disturbed Stress Field Model (Vecchio, 2000). Following the framework of Farag et al. (2024), each specimen was represented as a single four-node membrane element with smeared reinforcement in both orthogonal directions. This modeling approach, referred to as the "single membrane element" method, has been adopted in prior studies (Susetyo et al., 2013; Carnovale, 2013; Chasioti, 2017) and allows efficient yet accurate simulation of shear response in thin panels. Shear forces were introduced through corner-applied nodal loads, and the element was supported at its lower corners with pin and roller constraints, closely replicating experimental boundary conditions as established in prior work (e.g., Galik and Calvi, 2023).

Steel reinforcement was modeled with fixed mechanical properties across all simulations: yield strength (f_{sy}) of 420 MPa, ultimate strength (f_{su}) of 520 MPa, Young's modulus (E_s) of 200,000 MPa, a strain-hardening threshold (ε_{sh}) of 0.010, and an ultimate strain (ε_u) of 0.15. The bond between steel bars and the surrounding PFRC matrix was modeled using the default perfect bond assumption in VecTor2, though more detailed approaches are available (Zhang et al., 2024).

Fibers were modeled using a smeared reinforcement formulation as well, with assigned properties as follows: length = 40 mm, aspect ratio = 90, modulus of elasticity = 9,577 MPa, tensile strength = 620 MPa, and an equivalent diameter of 0.43 mm. These properties were chosen based on the work of Gaston (2023), who adopted GCP Strux 90/40. To capture crack development, the maximum crack spacing was set to 70 mm in both directions, based on prior experimental findings (Gaston, 2023), which have shown that this parameter is largely insensitive to changes in fiber content (Farag et al., 2024). All constitutive material models were defined as recommended by Farag et al. (2024) to maximize predictive accuracy.

 doi:10.20944/preprints202509.0760.v1

5.2. Numerical Analysis Key Results and Observed Trends

Key trends and insights derived from the numerical parametric study are presented in this section. Figure 4 illustrates representative shear stress–strain curves for selected panel configurations. These results correspond to panels with two levels of concrete compressive strength (45 MPa and 70 MPa), subjected to four transverse reinforcement ratios (0%, 0.1%, 0.5%, and 1.0%) and fiber contents ranging from 0% to 2% in 0.5% increments. In general, an increase in either transverse reinforcement or fiber content led to higher peak shear stresses, while the ultimate shear strain decreased. Fiber additions up to 0.5% by volume contributed modestly to peak strength but provided noticeable enhancements in ductility. These outcomes are in line with previous experimental findings (Navas et al., 2018; Gaston, 2023). An exception to this behavior was observed in panels without shear reinforcement, where even small volumes of fiber improved both shear resistance and post-peak deformation capacity.

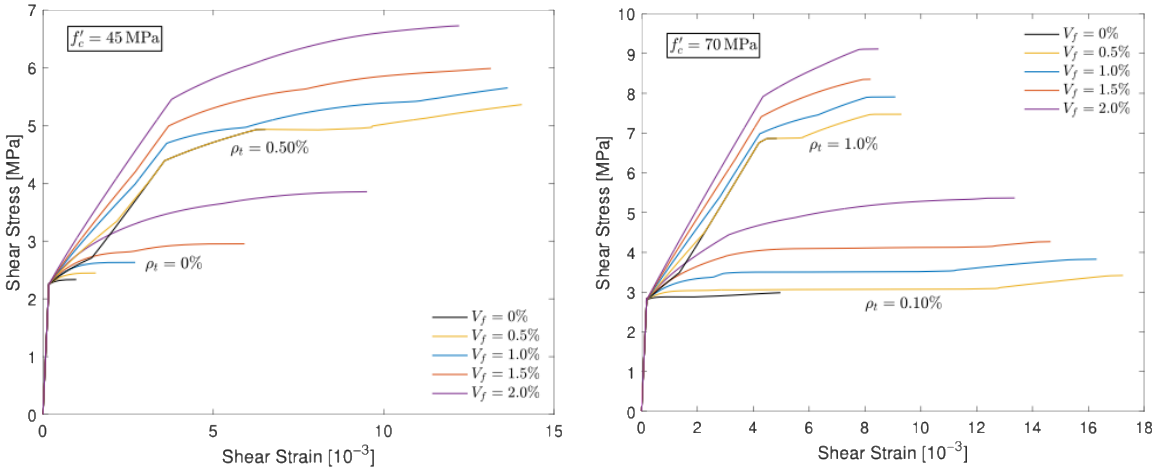

Figure 4. Typical shear Stress-Strain response as a function of transverse reinforcement and fiber content.

The strength gains achieved through fiber inclusion are further quantified in Figure 5, which plots the relative increase in shear capacity for various levels of fiber dosage, concrete strength, and shear reinforcement. Shear enhancement was defined as the ratio of the fiber-reinforced panel strength to that of an otherwise identical specimen lacking fibers. The analysis revealed that panels with higher concrete compressive strength ($f'_c \geq 70$ MPa) exhibited more substantial relative strength gains from fiber inclusion than panels with lower strength ($f'_c \leq 40$ MPa). Additionally, the marginal benefit of fiber reinforcement diminished in specimens with dense shear reinforcement ($\varrho_t > 0.75\%$), whereas panels with light or no shear reinforcement ($\varrho_t \leq 0.5\%$) showed the most pronounced improvement. Within the experimental bounds explored by Gaston (2023), where V_f did not exceed 0.52%, shear capacity gains remained under 10%, which aligns with the lack of a clear strength trend in that study. Notably, the greatest percentage increases were observed in lightly reinforced panels (e.g., $\varrho_t = 0.1\%$ and 0.25%), even exceeding those with no reinforcement at all. This suggests a potential synergistic effect between minimal bar reinforcement and fiber addition. Overall, fiber effectiveness declined as the transverse reinforcement increased, regardless of concrete grade.

 doi:10.20944/preprints202509.0760.v1

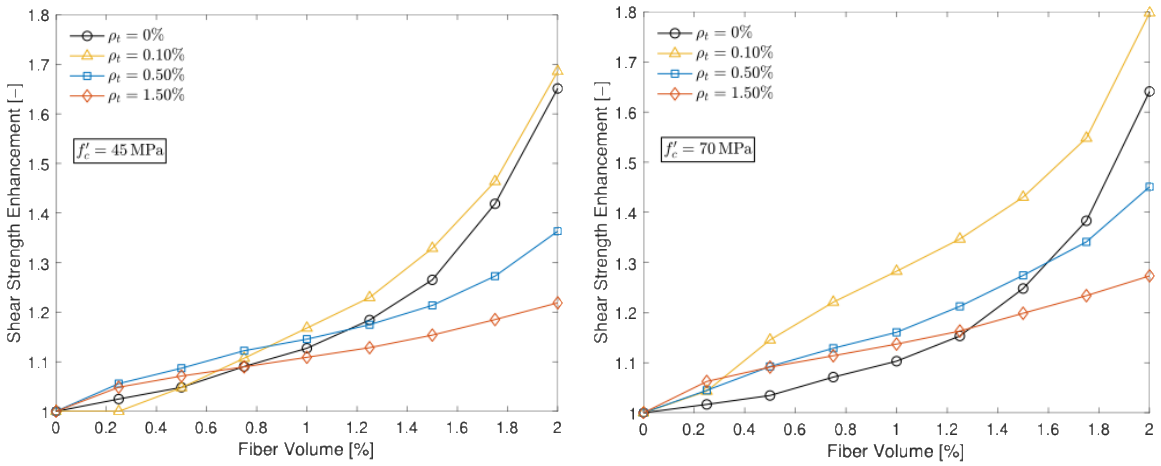

Figure 5. Typical shear strength increment for varying concrete strength and reinforcement ratio.

Figure 6 presents contour plots of computed shear strength (in MPa) as a function of transverse reinforcement ratio (ϱ_t) and fiber content (V_f) for concrete strengths of 45 MPa and 70 MPa. While the overall trends are consistent across all concrete grades, the magnitude of shear capacity naturally increases with higher compressive strength. The plots clearly show that both parameters positively influence shear strength, although the rate of increase varies. A mild interaction between ϱ_t and V_f is observable, though it has limited impact on the overall contour shapes. For instance, to achieve a target shear strength of approximately 5 MPa, the introduction of fibers at $V_f \approx 1.5\%$ allowed a significant reduction (nearly 50%) in required transverse bar reinforcement.

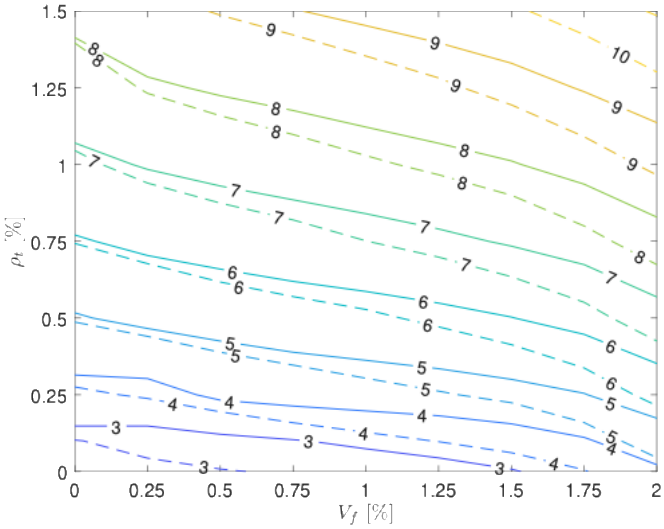

Figure 6. Influence of reinforcement ratio and fiber content on shear strength for varying concrete strength (f'_c = 45 MPa – solid line; f'_c = 70 MPa – dashed line).

Maximum crack widths corresponding to a normalized shear stress level of $0.4\sqrt{f'_c}$ (MPa) are shown in Figure 7, plotted against both ϱ_t and V_f. This stress level was chosen to display post-cracking crack widths as the cracking stress was $0.33\sqrt{f'_c}$ (Farag, 2024). Some models, particularly those without reinforcement and those with $\varrho_t = 0.125\%$, did not reach this stress level and are omitted from the plot. Overall, as observed in experimental studies (e.g., Gaston, 2023), increasing either the fiber content or the shear reinforcement ratio led to narrower cracks at the reference stress level. However, the impact of fiber inclusion on limiting crack widths became less significant as the amount of bar reinforcement increased, suggesting a complementary relationship between the two mechanisms of crack control.

 doi:10.20944/preprints202509.0760.v1

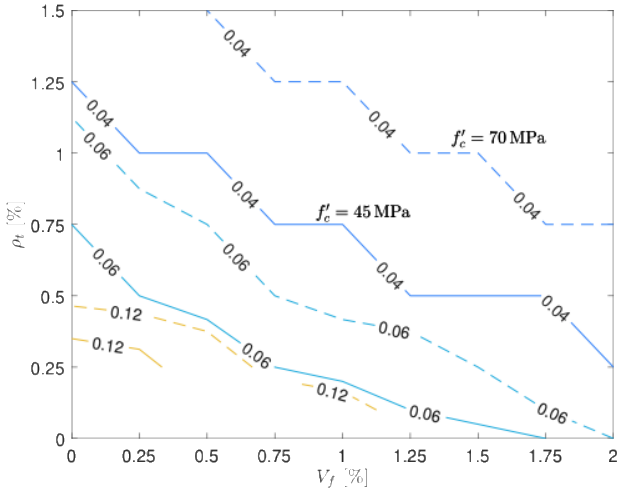

Figure 7. Crack widths at $v_{xy} = 0.4\sqrt{f'_c}$ for $f'_c = 45$ MPa (solid) and $f'_c = 70$ MPa (dashed).

6. Comparison of Available Design Methods with Parametric Study Results

The evaluation of the design codes presented in Section 3 is conducted mainly through the analysis of predicted-to-numerical strength ratios. A summary of these ratios, including their mean, median, and coefficient of variation (COV) values, for the entire parametric study is provided in Table 5. More detailed results can be found in Farag (2024).

The Fib Model Code exhibited the best overall performance, with an average prediction close to unity (Avg = 0.94), low scatter (Cov = 15.2%), and a narrow range of predicted-to-reference ratios (0.50 to 1.25

The AASHTO model was moderately conservative overall (Avg = 0.84), while having a greater scatter (Cov = 24.3%), and a maximum prediction of 1.21. It consistently underpredicted shear strength for high-strength concretes and at higher fibre contents but remained within acceptable bounds, making it a cautiously safe option.

In contrast, ACI and CSA models were consistently conservative across all specimen groups, with average predictions of 0.60 and 0.72, respectively. However, their scatter was substantial (Cov ~26–27%), and the lower bounds of predictions were as low as 0.20–0.22, suggesting that they may be overly penalizing the influence of fibres, especially at lower concrete strengths.

The EC2 models, particularly with cot(θ) = 1.0, provided the most conservative predictions (Avg = 0.44), often significantly underpredicting shear capacity, especially for specimens with higher fibre volumes. Although consistent in trend, this version yielded the lowest minimum prediction (0.12) and high variability (Cov = 35.8%). The EC2 with cot(θ) = 2.5 was more balanced in average prediction (Avg = 0.79) but showed the highest coefficient of variation (Cov = 43.8%), indicating high sensitivity to specimen parameters and significant inconsistency across the dataset.

Table 5. Predicted-to-numerical strength ratios for the parametric study.

Model code	Average	Median	COV [%]	Max [-]	Min [-]
AASHTO	0.84	0.88	24.3	1.21	0.34
ACI	0.60	0.62	26.5	0.97	0.22
Fib.	0.94	0.97	15.2	1.25	0.50
CSA	0.72	0.77	26.8	1.02	0.20

 doi:10.20944/preprints202509.0760.v1

EC2:					
cot(θ)=1.0	0.44	0.44	35.8	0.86	0.12
EC2:					
cot(θ)=2.5	0.78	0.73	43.7	1.69	0.26

The results summarized in Table 5 are also shown, somewhat more comprehensively, in Figure 8 which shows the code-predicted to VecTor2 (V_{VT2}) strength ratios. The predicted panel strength from the code equations considered versus the peak shear strength of the finite element models is outlined, grouping the results as a function of concrete strength. The dashed line indicates a 1:1 relationship.

As shown in the figure, model accuracy was affected by changes in concrete compressive strength, particularly when moving from lower-strength concretes (20–45 MPa) to high-strength concretes (70–95 MPa).

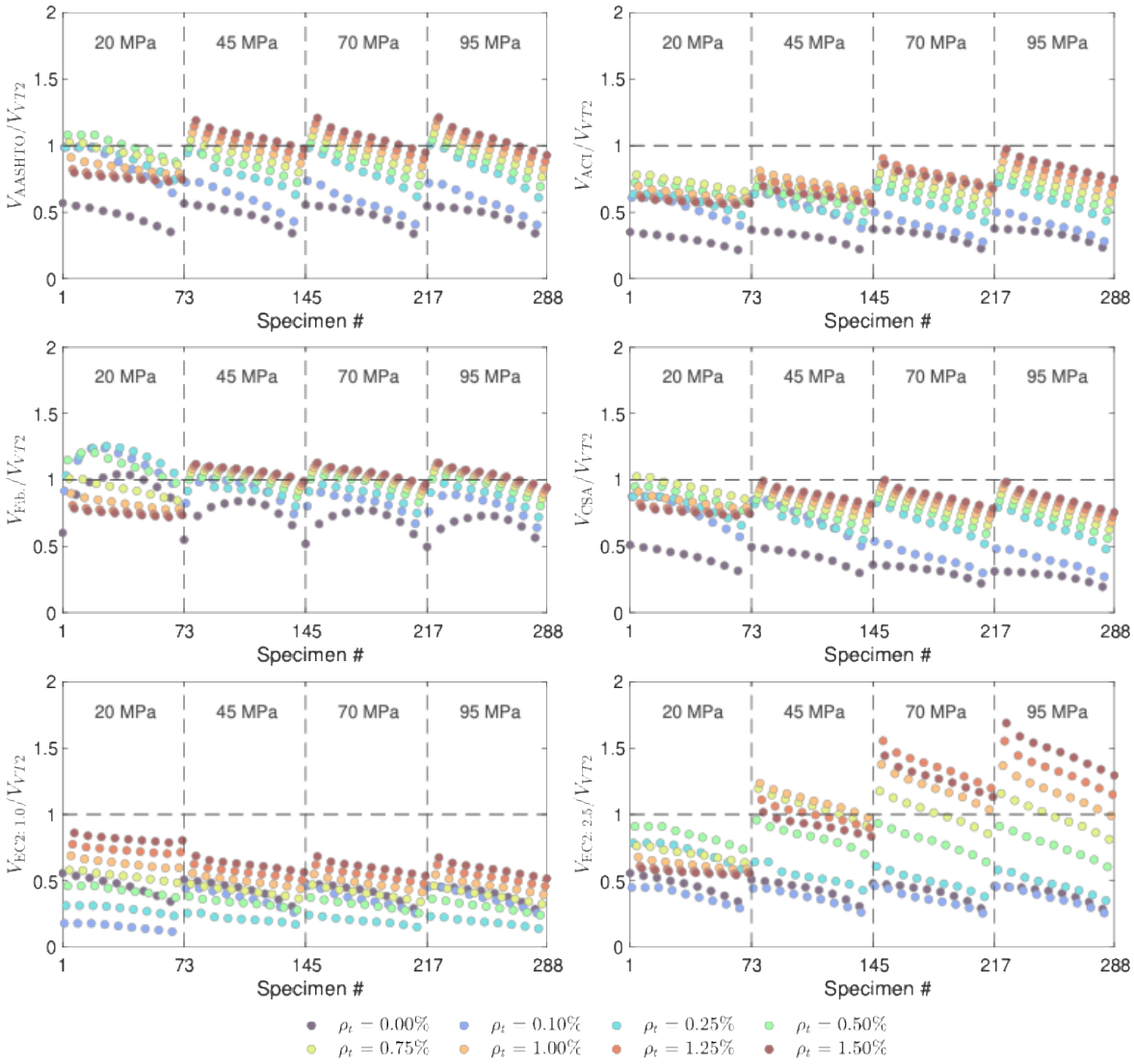

Figure 8. Code equation performance assessment against results from numerical parametric study.

At lower concrete strengths (20–45 MPa), most models (including ACI, CSA, and EC2) tend to perform more consistently, albeit conservatively. However, at higher concrete strengths (70–95 MPa),

 doi:10.20944/preprints202509.0760.v1

the performance of most models deteriorates. This is particularly apparent in the ACI and CSA models, whose predictions increasingly diverge from the reference values, resulting in more pronounced underestimations.

The EC2 models, although conservative across the board, also show growing scatter and prediction bias at higher strengths. For example, the EC2 with $\cot(\theta) = 1.0$ underpredicts shear strength significantly for higher-strength specimens.

In contrast, the Fib Model Code and AASHTO exhibit more favorable trends. The Fib model maintains consistent alignment with the reference predictions across all strength levels. Its underlying formulation accounts for a broader range of influencing parameters, including size effects and fibre contributions, which appear to provide better generalization across different strength classes. AASHTO, while generally underpredicting at higher strengths, shows a consistent slope in its response, suggesting that it could be recalibrated more easily than models with erratic performance.

This sensitivity to strength is critical because high-strength PFRC is increasingly used in structural applications where weight reduction and durability are prioritized. The results clearly indicate that most conventional models may not be reliably extrapolated to high-strength PFRC without adjustments.

The relative performance ranking of the models remains consistent with what discussed in Section 4, where the design models were assessed against the experimental results from the literature. This consistency strengthens confidence in the overarching conclusions regarding the inherent merits, limitations and tendencies of these models when applied to PFRC.

However, some differences arose in the degree of variability and sensitivity to parameters. For instance, in the experimental dataset, AASHTO was observed to significantly overpredict the shear strength of PFRC beams with shear reinforcement whereas in the parametric study, its predictions were generally conservative and more stable. This contrast may be attributed to the greater uniformity and control of variables in the parametric analysis, which reduces the scatter caused by complexities such as fibre distribution, detailing variations, and testing protocols that are inherent in experimental setups.

Perhaps most importantly, both the experimental and parametric analyses converge on the finding that model reliability deteriorates in the presence of shear reinforcement, where the combined action of fibres and transverse steel is not adequately addressed in most current formulations.

Overall, while the parametric study offered broader statistical confidence and consistency due to its controlled conditions, the outcome of the analyses reinforced the need for more targeted experimental research and model refinement to better capture the true behavior of PFRC elements, especially those incorporating both synthetic fibres and conventional reinforcement.

7. Conclusions and Recommendations for Future Work

This paper investigated the shear response of concrete elements reinforced by a combination of traditional steel reinforcement and synthetic fibers, focusing on assessing the reliability of available shear design methodology amongst existing code approaches. The experimental evidence currently available in the literature was first analyzed, but the limited amount of experimental data prevented the identification/development of design recommendations. Hence, an extensive parametric study was conducted in VecTor2, leveraging a recently developed numerical modeling approach for simulating the response of PFRC elements in shear. The parametric study extended the experimental results and explored the shear strength of PFRC panels with over 250 combinations of fiber contents, transverse reinforcement ratios, and concrete compressive strengths. Parameters of interest that were not tested in previous experimental programs were considered.

The ability of existing design code provisions to predict the shear strength of PFRC structural elements was then evaluated using the experimental data available, augmented by the numerical results from the parametric study.

The following key conclusions can be drawn:

 doi:10.20944/preprints202509.0760.v1

- The Fib Model Code emerged as the most reliable overall, showing the best balance between prediction accuracy and low variability in both the experimental and parametric datasets. Its formulation appears to generalize better across different geometries, strengths, and fibre contents.
- The AASHTO model performed reasonably well in both the parametric study and the experimental cases, but displayed some criticalities, especially for beams with shear reinforcement. This highlights potential calibration issues under combined fibre–steel action.
- ACI and CSA models were consistently conservative, with underestimations that became more pronounced at higher concrete strengths. While this may offer safety margins, it could lead to uneconomical designs in PFRC applications.
- The EC2 models with fixed cotangent angles, exhibited the highest variability and least reliability, especially in the presence of fibres. These models may not be suitable for FRC without significant modifications.
- The influence of concrete compressive strength was found to be significant. Many models underperformed at higher strengths (≥70 MPa), underscoring the need for strength-sensitive formulations.

While the parametric analysis offered broader statistical insight, the conclusions drawn from experimental data remain constrained by the limited number and heterogeneity of available tests. As such, the results of this study should be interpreted as indicative rather than definitive.

Future research efforts should consider the expansion of experimental datasets, particularly for PFRC elements with shear reinforcement, to better characterize the fibre–steel interaction and validate existing models under realistic conditions. The need for the development of unified models also persists. These should explicitly account for the synergistic effects of fibres and traditional reinforcement, as well as variable concrete strength and fibre distribution.

Acknowledgments: The authors would like to extend special appreciation to the ABC-UTC and the U.S. Department of Transportation Office of the Assistant Secretary for Research and Technology for funding this project.

Appendix

Table A1. PFRC specimen assembled database.

Specimen ID	d (mm)	a/d	ρ_l (%)	ρ_t (%)	f'_c (MPa)	V_f (%)	l_f (mm)	AR	$v_{u,exp}$ (MPa)
B3	120	3.0	2.62	0.28	37.8	0.50	50	85	3.78
B6	120	3.0	2.62	-	43.9	0.50	50	85	2.39
B7	120	3.0	2.62	-	44.2	1.00	50	85	3.14
B8	120	3.0	2.62	-	43.1	1.50	50	85	2.89
P-WV-50-0.5	265	3.0	1.78	-	41.9	0.50	50	63	1.47
P-WV-50-0.75	265	3.0	1.78	-	39.0	0.75	50	63	1.79
P-WV-50-1.0	265	3.0	1.78	-	37.9	1.00	50	63	1.68

 doi:10.20944/preprints202509.0760.v1

Specimen ID	d (mm)	a/d	ρ_l (%)	ρ_t (%)	f'_c (MPa)	V_f (%)	l_f (mm)	AR	$v_{u,exp}$ (MPa)
L1-0.50	400	3.5	2.15	-	41.9	0.50	40	90	1.72
L1-0.75	400	3.5	2.15	-	41.9	0.75	40	90	1.93
L2-0.50	330	3.5	3.18	-	41.9	0.50	40	90	1.75
L2-0.75	330	3.5	3.18	-	41.9	0.75	40	90	1.84
L2-1.0	330	3.5	3.18	-	35.6	1.00	40	90	2.00
Sh2-0.50	330	2.3	3.18	-	41.9	0.50	40	90	2.09
Sh2-0.75	330	2.3	3.18	-	41.9	0.75	40	90	2.23
Sy4.5-1	270	1.5	1.16	-	46.3	0.49	50	71	3.55
Sy4.5-2	270	2.5	1.16	-	46.3	0.49	50	71	2.03
PFRC	172	5.2	2.34	-	37.6	1.00	12.5	25	1.49
W510PFRC	255	2.5	1.24	-	26.0	1.45	40	53.3	2.24
W650PFRC	215	3.0	1.15	-	26.0	1.45	40	53.3	2.17
W770PFRC	255	2.5	1.23	-	26.0	1.45	40	53.3	2.29
W890PFRC	295	2.2	1.23	-	26.0	1.45	40	53.3	2.23
B2.5P1.0	210	2.5	1.28	-	27.0	1.00	39	51	1.52
B2.5P2.0	210	2.5	1.28	-	13.9	2.00	39	51	1.36
B2.5P3.0	210	2.5	1.28	-	18.5	3.00	39	51	1.78
B3.5P1.0	210	3.5	1.28	-	27.0	1.00	39	51	1.48
B3.5P2.0	210	3.5	1.28	-	13.9	2.00	39	51	1.35
B3.5P3.0	210	3.5	1.28	-	18.5	3.00	39	51	1.61
B4.5P1.0	210	4.5	1.28	-	27.0	1.00	39	51	1.24

 doi:10.20944/preprints202509.0760.v1

Specimen ID	d (mm)	a/d	ρ_l (%)	ρ_t (%)	f'_c (MPa)	V_f (%)	l_f (mm)	AR	$v_{u,exp}$ (MPa)
B4.5P2.0	210	4.5	1.28	-	13.9	2.00	39	51	0.99
B4.5P3.0	210	4.5	1.28	-	18.5	3.00	39	51	1.10
B1V3S0	125	2.4	3.22	-	44.4	0.33	40	90	2.56
B1V5S0	125	2.4	3.22	-	45.1	0.55	40	90	2.80
B1V7S0	125	2.4	3.22	-	45.9	0.77	40	90	3.08
OAP1	473	3.9	1.67	-	43.1	1.10	48	56	1.55
OAP2	473	4.8	2.23	-	44.9	1.10	48	56	1.69
OBP1	471	3.9	2.24	-	42.7	1.10	48	56	1.68
OBP2	469	4.9	2.25	-	42.0	1.10	48	56	1.38
AP1	475	3.9	1.67	0.10	44.0	1.10	48	56	2.40
AP2	474	4.8	2.23	0.10	44.6	1.10	48	56	2.34
BP1	481	3.8	2.19	0.15	45.0	1.10	48	56	2.52
BP2	475	4.8	2.22	0.15	44.2	1.10	48	56	2.24
HSC-0.75%S1-15M-0	201	3.7	1.41	-	71.4	0.75	50	74	2.23
HSC-0.75%S1-15M-S	201	3.7	1.41	0.50	57.0	0.75	50	74	2.06
HSC-0.75%S1-20M-0	199	3.7	2.53	-	78.3	0.75	50	74	3.42
HSC-0.75%S1-20M-S	199	3.7	2.53	0.50	89.2	0.75	50	74	3.14
HSC-0.75%S1-No.5(HS)-S	199	3.7	1.60	-	91.6	0.75	50	74	4.28
P2	225	1.7	1.19	-	45.3	0.22	54	68	2.19
P4	225	1.7	1.19	-	40.8	0.44	54	68	1.71
P8	225	1.7	1.19	-	37.7	0.88	54	68	2.07

 doi:10.20944/preprints202509.0760.v1

Specimen ID	d (mm)	a/d	ρ_l (%)	ρ_t (%)	f'_c (MPa)	V_f (%)	l_f (mm)	AR	$v_{u,exp}$ (MPa)
RC 2.5	225	3.1	0.47	-	56.3	0.27	48	56	1.81
RC 4.0	225	3.1	0.47	-	55.3	0.44	48	56	1.84
RC 5.5	225	3.1	0.47	-	54.8	0.60	48	56	1.96

References

AASHTO. (2007). *AASHTO LRFD Bridge Design Specifications* (4th ed.). American Association of State Highway and Transportation Officials, Washington, DC.

ACI Committee 318. (2019). *Building Code Requirements for Structural Concrete (ACI 318-19) and Commentary*. American Concrete Institute, Farmington Hills, MI, USA.

ACI Committee 544. (2018). *Guide to Design with Fiber-Reinforced Concrete (ACI 544.4R-18)*. American Concrete Institute, Farmington Hills, MI.

Ababneh, A., Al-Rousan, R., Alhassan, M., & Alqadami, M. (2017). Influence of synthetic fibers on the shear behavior of lightweight concrete beams. *Advances in Structural Engineering*, 20(11), 1671–1683.

AbdelAleem, B. H., Ismail, M. K., & Hassan, A. A. (2018). The combined effect of crumb rubber and synthetic fibers on impact resistance of self-consolidating concrete. *Construction and Building Materials*, 162, 816–829.

Alhassan, M., Al-Rousan, R., & Ababneh, A. (2017). Flexural behavior of lightweight concrete beams encompassing various dosages of macro synthetic fibers and steel ratios. *Case Studies in Construction Materials*, 7, 280–293.

Altoubat, S., Yazdanbakhsh, A., & Rieder, K.-A. (2009). Shear behavior of macro-synthetic fiber-reinforced concrete beams without stirrups. *ACI Materials Journal*, 106(4). https://doi.org/10.14359/56659

Amin, A., & Foster, S. J. (2015). Shear strength of steel fibre reinforced concrete beams with stirrups. *Engineering Structures*, 111, 323–332.

Aoude, H., Belghiti, M., Cook, W. D., & Mitchell, D. (2012). Response of steel fiber-reinforced concrete beams with and without stirrups. *ACI Structural Journal*, 109(3), 359–368.

Arslan, G., Keskin, R. S. O., & Ozturk, M. (2017). Shear behaviour of polypropylene fibre-reinforced-concrete beams without stirrups. *Proceedings of the Institution of Civil Engineers – Structures and Buildings*, 170(3), 190–198.

Bastami, R. (2019). *Structural performance of high-strength reinforced concrete beams built with synthetic fibers* (Doctoral dissertation). University of Ottawa.

Bentz, E. C., Vecchio, F. J., & Collins, M. P. (2006). Simplified modified compression field theory for calculating shear strength of reinforced concrete elements. *ACI Structural Journal*, 103(S65), 614–624.

Carnovale, D. J. (2013). *Behaviour and analysis of steel and macro-synthetic fibre reinforced concrete subjected to reversed cyclic loading: A pilot investigation* (Master's thesis). University of Toronto.

Carnovale, D., & Vecchio, F. J. (2014). Effect of fiber material and loading history on shear behavior of fiber-reinforced concrete. *ACI Structural Journal*, 111(5), 1235–1244.

Chasioti, S. (2017). *Hybrid steel fibre reinforced concrete in shear: From the material to the structural level* (Doctoral dissertation). University of Toronto.

 doi:10.20944/preprints202509.0760.v1

Conforti, A., Minelli, F., Tinini, A., & Plizzari, G. A. (2015). Influence of polypropylene fibre reinforcement and width-to-effective depth ratio in wide-shallow beams. *Engineering Structures*, 88, 12–21.

CSA (Canadian Standards Association). (2014). *Design of Concrete Structures* (CSA A23.3). Mississauga, ON, Canada.

Cucchiara, C., La Mendola, L., & Papia, M. (2004). Effectiveness of stirrups and steel fibres as shear reinforcement. *Cement & Concrete Composites*, 26(7), 777–786. https://doi.org/10.1016/j.cemconcomp.2003.07.001

Farag, D. F. (2024). Predicting The Shear Strength of Macro-Synthetic Fiber-Reinforced Concrete. Master's Thesis, University of Washington. https://hdl.handle.net/1773/52452

Farag, B. F., Thonstad, T., & Calvi, P. M. (2024). Numerical modeling of distributed macro-synthetic fiber and deformed bar reinforcement to resist shear. *Buildings*, 14(10), 3247. https://doi.org/10.3390/buildings14103247

fib (Fédération Internationale du Béton). (2010). *Model Code for Concrete Structures 2010*.

Galik, W. D., & Calvi, P. M. (2023). Shear strength of steel-concrete composite "NPS® Basic" truss beams. *Engineering Structures*, 290, 116362.

Gaston, J. P. (2023). *Shear behavior of macro-synthetic fiber-reinforced concrete panels* (Master's thesis). University of Washington, Seattle, WA.

Greenough, T., & Nehdi, M. (2008). Shear behavior of fiber-reinforced self-consolidating concrete slender beams. *ACI Materials Journal*, 105(5), 468–477.

Ismail, M. K., AbdelAleem, B. H., Hassan, A. A., & El-Dakhakhni, W. (2025, March). Shear behavior of lightweight engineered cementitious composite RC beams. In *Structures* (Vol. 73, p. 108403). Elsevier.

Hossain, F. Z., Pal, A., Ahmed, K. S., Bediwy, A., & Alam, M. S. (2023). Shear behavior of polypropylene fiber-reinforced concrete beams containing recycled aggregate and crumb rubber. *Journal of Cleaner Production*, 412, 137370.

Joshi, S. S., Thammishetti, N., & Prakash, S. S. (2018). Efficiency of steel and macro-synthetic structural fibers on the flexure-shear behaviour of prestressed concrete beams. *Engineering Structures*, 171, 47–55.

Karthik, M. P., & Maruthachalam, D. (2015). Experimental study on shear behaviour of hybrid fibre reinforced concrete beams. *KSCE Journal of Civil Engineering*, 19(1), 259–264.

Koura, M. M., Tahwia, A. M., & Matthana, M. H. (2024). Influence of macro-synthetic fibers on the flexural behavior of high strength concrete beams reinforced with GFRP bars. *Mansoura Engineering Journal*, 49(4), 4.

Majdzadeh, F., Soleimani, S. M., & Banthia, N. (2006). Shear strength of reinforced concrete beams with a fiber concrete matrix. *Canadian Journal of Civil Engineering*, 33(6), 726–734.

Murad, Y., & Abdel-Jabbar, H. (2022). Shear behavior of RC beams prepared with basalt and polypropylene fibers. *Case Studies in Construction Materials*, 16, e00835.

Navas, F. O., Navarro-Gregori, J., Herdocia, G. L., Serna, P., & Cuenca, E. (2018). An experimental study on the shear behaviour of reinforced concrete beams with macro-synthetic fibres. *Construction and Building Materials*, 169, 888–899.

Parmentier, B., Cauberg, N., & Vandewalle, L. (2012, September). Shear resistance of macro-synthetic and steel fibre reinforced concrete beams without stirrups. In *Proceedings of the 8th RILEM International Symposium on Fibre Reinforced Concrete*, Guimarães, Portugal (pp. 19–21).

Sahoo, D. R., Maran, K., & Kumar, A. (2015). Effect of steel and synthetic fibers on shear strength of RC beams without shear stirrups. *Construction and Building Materials*, 83, 150–155.

Susetyo, J., Gauvreau, P., & Vecchio, F. J. (2013). Steel fiber-reinforced concrete panels in shear: Analysis and modeling. *ACI Structural Journal*, 110(2), 285–294.

Swamy, R. N., & Bahia, H. M. (1985). The effectiveness of steel fibers as shear reinforcement. *Concrete International*.

Vecchio, F. J. (1990). Reinforced concrete membrane element formulations. *Journal of Structural Engineering*, ASCE, 116(3), 730–750.

Vecchio, F. J. (2000). Disturbed stress field model for reinforced concrete: Formulation. *Journal of Structural Engineering*, 126(9), 1070–1077.

Vecchio, F. J., & Collins, M. P. (1986). The modified compression-field theory for reinforced concrete elements subjected to shear. *ACI Journal Proceedings*, 83(2), 219–231. https://doi.org/10.14359/10416

Wong, P. S., Vecchio, F. J., & Trommels, H. (2013). *Vector2 & Formworks user's manual* (2nd ed.). University of Toronto, Canada.

Zhang, H., Calvi, P. M., Lehman, D., Kuder, K., & Roeder, C. (2020). Response of recycled coarse aggregate concrete subjected to pure shear. *Journal of Structural Engineering*, 146(5), 04020059.

Zhang, Z., & Gu, G. X. (2020). Finite-element-based deep-learning model for deformation behavior of digital materials. *Advanced Theory and Simulations*, 3(7), 2000031.